

Analysis of solid oxide fuel cell systems for off-grid energy production

Boudjemaa Mehimedetsi¹, Abdellah Draidi², Billel Smaani^{1,3}

¹Department of Electromechanical, Institute of Science and Technology, Abdelhafid Boussouf University Center, Mila, Algeria

²Department of Electromechanical, Institute of Applied Science and Technology, University of Constantine 1, Constantine, Algeria

³Laboratoire Hyperfréquences et Semiconducteurs, University of Constantine 1, Constantine, Algeria

Article Info

Article history:

Received May 15, 2024

Revised Mar 12, 2025

Accepted Jul 3, 2025

Keywords:

DC/DC converter

Dual controllers

Inverter

LCL filter

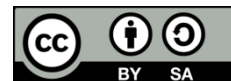
SOFC

Stand-alone generation

ABSTRACT

This work presents a simulation study of a 50-kW solid oxide fuel cell (SOFC) power supply system that provides electricity to residential users. Indeed, many decentralized applications rely on renewable energy sources not connected to the primary power grid. Moreover, fuel cell modelling and simulation are critical for promoting renewable energy as they eliminate the need for physical prototypes, saving time and money. We have also developed a reliable model for simulating self-contained SOFC fuel cells. The elaborated model includes the kinetics of electrochemical processes and accounts for voltage losses in SOFCs. Our fuel cells produce the necessary electrical current to charge the device. Also, our system has fuel cells, a DC/DC converter, and an inverter with LCL filters. These components connect the fuel cell system to other power electronics and the electrical load. Furthermore, a mathematical model of a dual inverter system describes its control method, including the proportional and integral parameters in the voltage and current loops has been derived. The proposed model and system could be helpful for a standalone load.

This is an open access article under the [CC BY-SA](https://creativecommons.org/licenses/by-sa/4.0/) license.



Corresponding Author:

Boudjemaa Mehimedetsi

Department of Electromechanical, Institute of Science and Technology

Abdelhafid Boussouf University Center

Mila, Algeria

Email: alihhas@upm.edu.my

1. INTRODUCTION

Most countries are trying to replace the generation of electrical energy created from polluting, rapidly depleted, complex, and expensive fossil fuels with other methods that are clean, reliable, and environmentally friendly. Renewable energy sources are at the center of political debates as a way to decrease our dependence on non-renewable fossil fuels [1]. Solid oxide fuel cells (SOFCs) are commonly used to generate electrical energy, and are continually studied and developed, they have high ionic conductivity, which improves their performance and efficiency by up to 60% and have many advantages such as being quiet, modular, easily adjusted to meet the power requirements of various applications, efficient in extracting electrical energy. The temperature range in which it operates is between 600 and 1,000 degrees Celsius. They are more efficient and sustainable than other fuel cell technologies. They use a hard ceramic substance, usually zirconium oxide with trace amounts of yttria, as a solid electrolyte. In addition, SOFC fuel cells use electrochemical processes instead of combustion, and do not emit pollutants. Their high fuel efficiency and performance make them ideal for electric vehicles and marine propulsion. They can be used in industry and sectors and help improve alternative energy sources as they can generate large amounts of energy or combine heat. Compared to other

forms of fuel cells, which require only pure hydrogen as a fundamental material, SOFC fuel cells can also use natural gas or biogas [2].

Fuel cell development is progressing toward creating clean energy, but challenges remain. Catalysts and electrolyte components degrade quickly, requiring the development of durable materials and techniques. Fuel cells to date have been expensive compared to conventional energy sources, which requires additional sound research in materials science, engineering and process design. Hydrogen has flammability problems, has low density, and takes a lot of storage and transport [3]-[5]. Fuel cells require precise planning and integration with power electronics, temperature and water management, and control systems for efficient integration into the power grid or an isolated load [6].

The fuel cell studies by several authors have shown the importance of using it off-grid or on-grid, alone or mixed with other energy sources. Vora and Williams [7], have presented the SOFC program of the US Department of Energy is developing low-cost, high-efficiency SOFC power generation systems. These systems have near-zero emissions, require less water, and can achieve over 60% efficiency. Reiter [8], discusses the automation of SOFC technology in South Africa, accent its potential for decentralized power generation and marine applications. Yang *et al.* [9], this review examines various control strategies for SOFCs to ensure efficiency, effectiveness, and reliability. The study divides the control methods into eight categories: proportional-integral-derivative (PID), advanced process control (APC), robust, model predictive control (MPC), fuzzy logic control (FLC), fault-tolerant control (FTC), intelligent, and observer-based. Lai and Adams [10], the study examined the effects of natural gas and coal content on the premature degradation of SOFCs power plants. It included four models: autonomous, steam, hybrid SOFC/GT and hybrid SOFC/GT. The result showed that the SOFC/GT hybrid is the best in plant and SOFC production efficiency. Liu *et al.* [11], this paper, the adaptive model predictive control (AMPC) algorithm is proposed for controlling SOFCs in a DC microgrid. The AMPC algorithm uses a parameter estimator to update the online system parameters, improving control performance and introducing less model dependence. Shin *et al.* [12], a study recommends the use of cascade design to improve the electrical efficiency of solid oxide fuel cell systems. It consists of two stacks installed in series, with the second stack using the anode off-gas from the first stack. Simulation results showed that the cascade scheme was the most effective, except for low external variable rates. Brunaccini *et al.* [13] this study is part of the European onsite project consist developed a simulation tool for hybrid fuel cell/battery design. That system will combine a solid oxide fuel cell with a high-temperature nickel-sodium chloride battery and study heat transfer from using hot gases to regulate energy flows. Tan *et al.* [14], the purpose of this paper is to examine the application field of SOFC in buildings, focusing on system design concepts, performance evaluations and forecasting models, building load calculation as well as strategies for improving SOFC systems. Baldi *et al.* [15] the proposed hybrid CHP system uses a mixed integer linear optimization concept to integrate a SOFC as the main generator with hydrogen storage in a purification unit. Such technology is used in self-sufficient residential and leisure yachts to reduce capital costs while maintaining SOFC as the main energy source. Gelen and Yalcinoz [16], this paper, a new thermal-based modified dynamic model of SOFC for grid-connected applications is developed. Ro and Rahman [17], have presented a new method for controlling fuel cell devices in an electric utility distribution network. They proposed an approach that aimed at enhancing the stability and efficiency of the power supply by making it robust and responsive while minimizing generator oscillations. Li *et al.* [18], solution is designed for adjusting the power output of a solid oxide fuel cell power plant when connected to an AC grid. In addition, this work can be useful practically as it tries to improve generation and use of energy with specific focus on how dynamic behavior should be understood as well as control mechanisms so that optimum efficiency can be achieved. Sergi *et al.* [19], The work suggests a robust PI controller that offers optimal active power regulation of SOFC systems for secure and reliable operation.

The research concentrates on improving the efficiency of SOFC systems through inverter control strategies. The system, which consists of two controllers for voltage and current, improves system stability and power quality, particularly in off-grid situations. It has excellent scaling and configurability, covering power outputs from 5 kW to 50 kW. The system uses an optimization method to increase overall efficiency beyond the current benchmark under operating loads. The study aims to inspire further technologies to increase the efficiency of power generation, thereby improving the quality of life for all. It provides detailed visions into modelling strategies, system components, performance evaluation and recommendations for SOFC systems for off-grid power systems.

2. LITERATURE REVIEW

2.1. Fuel cell classification

Fuel cells run at low temperatures (60 °C and 250 °C) and high temperatures (600 °C and 1,000 °C) and use combustible materials. There are some types: proton exchange membrane fuel cell (PEMFC), direct

methanol fuel cell (DMFC), phosphoric acid fuel cell (PAFC), alkaline fuel cell (AFC), molten carbonate fuel cell (MCFC) and SOFC [7], [8].

Figure 1 shows a graph comparing different types of fuel cells based on their operating temperature range and power output. Fuel cells convert fuel into direct current through an electrochemical reaction. They consist of two electrodes separated by a membrane and an electrolyte. Fuel and oxygen mix into the electrolyte, react and generate electricity. Due to the low voltage developed by a single fuel cell, multiple cells are required to create enough power [20].

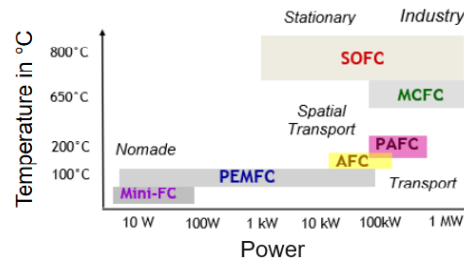


Figure 1. Fuel cells different types characteristics [21]

2.2. Description of the SOFC fuel cells

Fuel cells convert fuel into DC through electrochemical process. They consist of two electrodes separated by a membrane and an electrolyte. The fuel and gaseous oxygen are introduced into the electrolyte, where they react to generate electricity. Due to the low voltage developed by a single fuel cell, multiple cells are required to create enough power [20].

At the anode: $\text{H}_2 \rightarrow 2\text{H}^+ + 2\text{e}^-$

At the cathode: $\text{O}_2 + 4\text{H}^+ + 4\text{e}^- \rightarrow 2\text{H}_2\text{O}$

Figure 2 shows that hydrogen (H_2) is oxidized at the anode in this reaction to produce protons (H^+) and electrons (e^-). The electrons are directed through an external circuit to generate electrical energy. Meanwhile, oxygen (O_2) is reduced to form water at the cathode (H_2O).

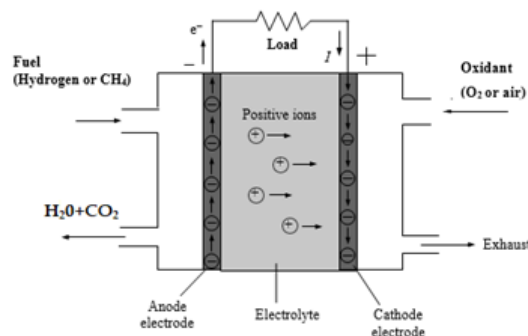


Figure 2. SOFC schematic

2.3. Modeling of the solid oxide cell

A SOFC is affected by various factors such as temperature, airflow, and fuel flow. These factors affect results such as emissions, efficiency, and electricity production. The process of how this works is complicated and complex, meaning that a change to one part can affect many other parts. [22], [23]. Solid oxide fuel cell modeling uses several models (0-D, 1-D, 2-D, 3-D) with advantages and disadvantages. Other research proposes electrochemical impedance spectroscopy (EIS) to study the behavior of fuel cells. Researchers use experimental data and electrochemical models such as the Butler-Volmer equation to develop fuel cell models. Computational fluid dynamics (CFD) is used to analyze mass, momentum, and energy flows [22]-[31]. In this, we addressed MATLAB modeling and the influence of voltage, current, and power density on the efficiency of the selected fuel cells concerning the operating conditions and the materials. The important factors include current flowing, temperature and hydrogen partial pressures, which are important for every electrochemical process [32]-[35].

$$\frac{dp_{H_2}}{dt} = \frac{1}{\tau_{H_2}} \left[\frac{1}{k_{H_2}} (q_{H_2}^{in} - 2K_r i_{fc}) - p_{H_2} \right] \quad (1)$$

$$\frac{dp_{O_2}}{dt} = \frac{1}{\tau_{O_2}} \left[\frac{1}{k_{O_2}} (q_{O_2}^{in} - K_r i_{fc}) - p_{O_2} \right] \quad (2)$$

$$\frac{dp_{H_2O}}{dt} = \frac{1}{\tau_{H_2O}} \left[\frac{1}{k_{H_2O}} 2K_r i_{fc} - p_{H_2O} \right] \quad (3)$$

where;

$p_{H_2}, p_{O_2}, p_{H_2O}$ denote the partial pressure values of hydrogen, oxygen and water in *atm*, respectively.

$q_{H_2}^{in}, q_{O_2}^{in}$: incoming molar hydrogen, and oxygen flow rate *kmol/s*

$k_{H_2}, k_{O_2}, k_{H_2O}$ respectively fuel, air, and fuel exhaust valves molar constant, *Kmol s/atm*

$\tau_{H_2}, \tau_{O_2}, \tau_{H_2O}$ respectively fuel, air, and fuel exhaust valves time constant, *s*

i_{fc} fuel cell DC current, *A*, $K_r = \frac{N_0}{4F}$ is a modeling constant, *Kmol/sA*, *F* Faraday's constant *C/kmol*

The output voltage of a SOFC is determined in the (8) by deducting three principal losses: ohmic losses (ion and electron transport) arising from internal resistance:

$$V_{ohmic} = i_{fc} R_{fc} \quad (4)$$

Activation losses associated with reaction kinetics:

$$V_{activation} = A \ln \frac{i_{fc}}{i_0} \quad (5)$$

$A = \frac{RT}{2\alpha F}$ is a constant in the Tafel equation, with *R* is the gas constant, *T* is the temperature, α as the charge transfer coefficient, and concentration overvoltage (mass transfer losses) can be modeled using Fick's law, which accounts for diffusion and limiting current density i_l

$$V_{concentration} = \frac{RT}{nF} \ln \left(\frac{i_l}{i_l - i_{fc}} \right) \quad (6)$$

The theoretical maximum voltage in a fuel cell as defined by the Nernst equation:

$$E_{fc} = N_0 \left(E_0 + \frac{RT}{2F} \left[\ln \frac{p_{H_2} p_{O_2}^{\frac{1}{2}}}{p_{H_2O}} \right] \right) \quad (7)$$

In this context E_{fc} signifies the theoretical cell voltage E_0 , represents the standard potential or open-circuit voltage, denotes the gas constant (8.314 J/(kmol·K)), indicates temperature in Kelvin, and stands for Faraday's constant (96485 C/mol), N_0 number of cells; Increased hydrogen consumption generally elevates cell voltage; likewise, augmented oxygen content improves performance. In contrast, sensitive water vapor generation decreases the working pressure within the stack [35], [36], [37].

$$V_{fc} = E_{fc} - V_{ohmic} - V_{activation} - V_{concentration} \quad (8)$$

Fuel utilization efficiency [36], [38], which indicates the effectiveness of hydrogen input conversion into electrical energy, is directly associated with the current density passing through the fuel cell:

$$U_f = \frac{q_{H_2}^{in} - q_{H_2}^o}{q_{H_2}^{in}} = \frac{q_{H_2}^r}{q_{H_2}^{in}} = \frac{n I_{fc}}{2 F q_{H_2}^{in}} \quad (9)$$

where i_{fc} denotes the cell current and *n* number of electrons transferred per molecule of hydrogen in the electrochemical reaction.

Figure 3 shows the voltage (V/cell) versus current density (A/cm²). It shows three distinct regions: activation losses at low current density, ohmic losses at medium density, and concentration losses at high current density. Table 1 illustrates the parameters of the fuel cell used; Figure 4 shows the different blocks of the fuel cell implemented in MATLAB/Simulink.

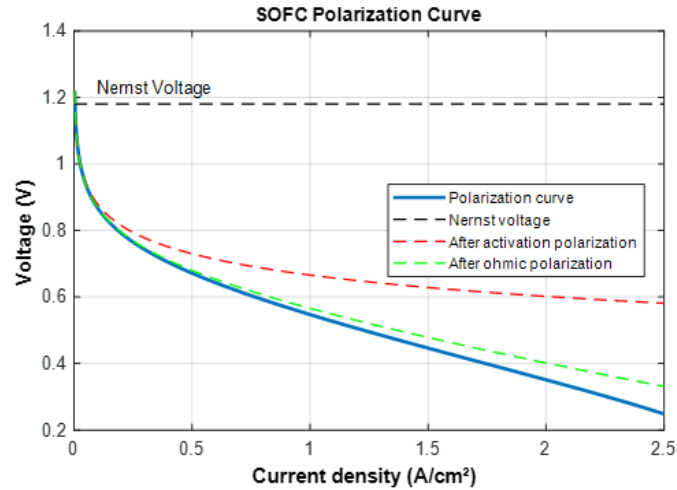


Figure 3. SOFC polarization curve

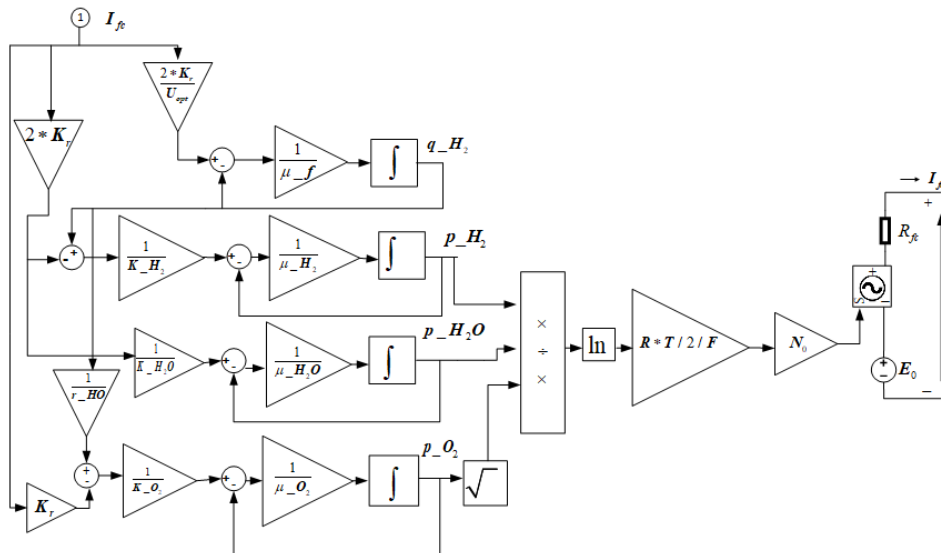


Figure 4. Dynamic model of SOFC developed in MATLAB/SIMULINK

Table 1. The parameters of the fuel cell SOFC

Parameter	Representation	Value
P_{rate}	Rated power	50 kW
T	Absolute temperature	1273 K
F	Faraday's constant	96487 C/mol
R	Universal gas constant	8.314 J/(kmolK)
E_0	Ideal standard potential	1.18 V
N_0	Number of cells in series in the stack	450
$K_r = N_0/4F$	Constant kmol/(sA)	0.996×10^{-6}
$U_{max}, U_{min}, U_{opt}$	Maximum, minimum, optimal fuel utilization	[0.9 0.8 0.85]
K_H	Valve molar constant for hydrogen kmol/(s atm)	8.43×10^{-4}
K_{H_2O}	Valve molar constant for water kmol/(satm)	2.81×10^{-4}
K_{O_2}	Valve molar constant for oxygen kmol/(satm)	2.52×10^{-3}
τ_{H_2}	Response time for hydrogen flow	26.1 s
τ_{H_2O}	Response time for water flow	78.3 s
τ_{O_2}	Response time for oxygen flow	2.91 s
r	Ohmic loss	$3.28 \times 10^{-4} \Omega$
T_e	Electrical response time	0.8 s
T_f	Fuel processor response time	5 s
r_{H_2O}	Ratio of hydrogen to oxygen	1.145

3. OVERALL STAND-ALONE LOAD MODELING

Figure 5 shows the block diagrams of the modeled system, while Figure 6 shows the entire electrical circuit. Boost DC/DC converters, filter circuits, and inverters are commonly used to convert DC power to AC power for fuel cells. The operation is performed using PI controllers for current and voltage.

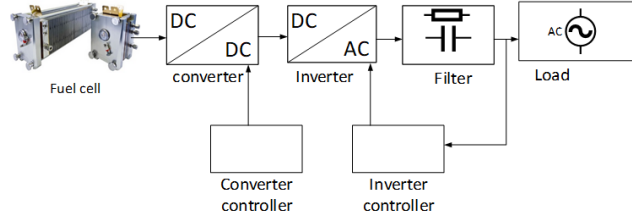


Figure 5. Block diagram of the entire system

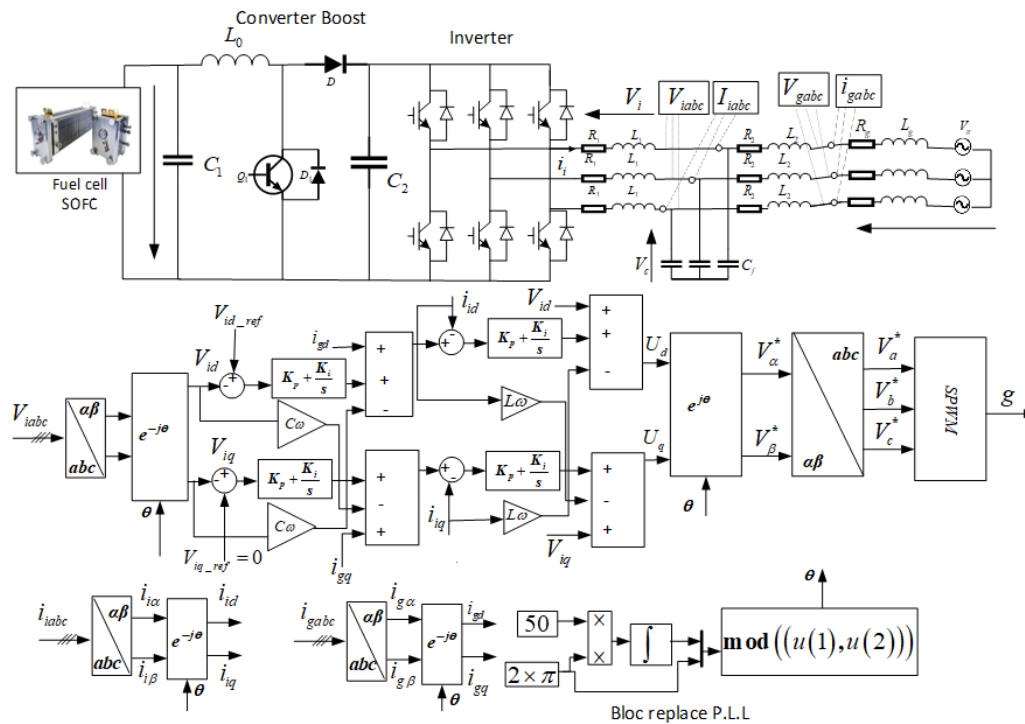


Figure 6. Schematic of the fuel cell off grid with control

3.1. DC boost converter

The SOFC fuel cell requires a DC-DC converter to function correctly. The converter's main purpose is to increase the voltage required for the DC-AC converter and load requirements. As the chemical reactions in fuel cells are progressive, a DC-DC boost converter is needed at the output terminal. The circuit cited in Figure 7 contains an inductor, switch, diode, and capacitor. The switch can be either a MOSFET or IGBT semiconductor. The duty cycle d can regulate the output voltage.

$$V_{out} = V_{in} \left(\frac{T_{on} + T_{off}}{T_{off}} \right) = V_{in} \left(\frac{T}{T_{off}} \right) = \frac{1}{1-d} V_{in} \quad (10)$$

- $(0 < t \leq t_{on})$ mode: the switch S is closed during the initial operation phase, and the input voltage charges the inductor, which stores energy.
- $(t_{on} < t < T_s)$ mode: when switch S opens during the second phase, the inductor discharges into the load via the diode.

The state-space model in continuous conduction mode (CCM), is given by (11) [37].

$$\frac{d}{dt} \begin{bmatrix} i_L \\ v_C \end{bmatrix} = \begin{bmatrix} 0 & -\frac{1-d}{L} \\ \frac{1-d}{C} & -\frac{1}{RC} \end{bmatrix} \begin{bmatrix} i_L \\ v_C \end{bmatrix} + \begin{bmatrix} \frac{1}{L} \\ 0 \end{bmatrix} v_i \quad (11)$$

L and C values are calculated by (12) and (13) respectively

$$L_{max} = \frac{0.25 V_O T}{\Delta i_L} \quad (12)$$

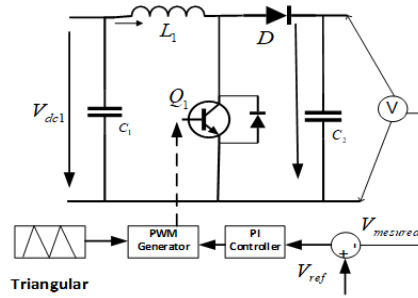


Figure 7. Boost converter

where:

$$\Delta i_L = 20\% I_0 \quad (13)$$

$$C_{min} = \frac{\Delta i_L}{8 f \Delta V_{Cmax}} \quad (14)$$

where:

$$\Delta V_{Cmax} = \Delta V_{0max} = 0.1\% V_0 \quad (15)$$

3.2. LCL filter

The system uses an LCL filter, illustrated in Figure 8, to enhance the power quality of the load by removing any ripples in the inverter's voltage output. This filter consists of resistors, capacitors, and inductors in Figure 8(a) without a resistor damper or an added series resistor damper with capacitors in Figure 8(b). Generally, filter LCL minimizes the impact of electrical disturbances on the inverter by managing oscillations, controlling the circuit's switching frequency, and regulating the voltage supply.



Figure 8. LCL filter (a) without resistor damper and (b) with series resistor damper

The design specifications for the LCL filter require frequency domain computation of switching ripple attenuation, and the filter values are reported as a percentage of base values [39]-[41].

$$Z_b = \frac{(E_n)^2}{S_n} \quad (16)$$

$$C_b = \frac{1}{\omega_n Z_b} \quad (17)$$

E_n is the efficacy voltage between lines, ω_n is the load or grid frequency, S_n is the rated active power absorbed by the converter.

The transfer function $H_{LCL}(s)$ with damping resistor is,

$$H_{LCL}(s) = \frac{i_n}{v_i} = \frac{C_f R_f s + 1}{L_1 C_f L_2 s^3 + C_f (L_1 + L_2) R_f s^2 + (L_1 + L_2) s} \quad (18)$$

The system's power factor variation is estimated to be 5% for the filter capacity design. This causes a modification in the system's base impedance, where in,

$$C_f = 0.05 C_b \quad (19)$$

Tolerable current ripple on the side converter,

$$\Delta I_{lmax} = 0.1 \left(\frac{\sqrt{2} S_n}{E_n} \right) \quad (20)$$

For the design norms, the rated current is permitted to vary by 10%.

$\Delta I_{lmax} = 10\% I_{max}$ Inverter-side inductance

$$L_1 = \frac{E_n}{6 f_{sw} \Delta I_{lmax}} \quad (21)$$

Grid-side inductance,

$$L_2 = 1.2 L_1 \quad (22)$$

Resonance pulsation,

$$\omega_{res} = \sqrt{\frac{L_1 + L_2}{L_1 L_2 C_f}} \quad (23)$$

Filter's resonance frequency,

$$f_{res} = \frac{\omega_{res}}{2\pi} \quad (24)$$

Damping resistance,

$$R_d = \frac{1}{3 \omega_{res} C_f} \quad (25)$$

The bode criteria in the Figure 9 are utilized to analyze a filter's amplitude and phase characteristics, which provides essential insights into signal synchronization, gain, and frequency-dependent phase shift. It is crucial to comprehend this information to evaluate the filter's behavior and make informed decisions about its design and operation.

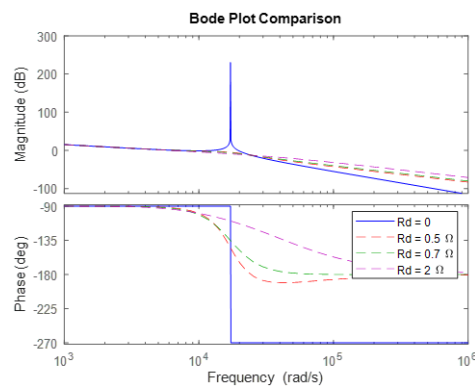


Figure 9. Bode of Rd-Cd damped LCL filter

3.3. DC/AC inverter

The inverters convert the DC power received from a boost converter into AC power, as shown in Figure 10. The output voltage and frequency are modified to match the load. Two-axis reference frame dual control inverters regulate load voltage and current by transforming three-phase AC and voltage. These inverters are capable at cost-effectively regulating the output voltage and frequency to satisfy the load [42].

$$\begin{aligned} V_{sR} &= \frac{1}{3} V_{dc} (2s_1 - s_2 - s_3) \\ V_{sS} &= \frac{1}{3} V_{dc} (-s_1 + 2s_2 - s_3) \\ V_{sT} &= \frac{1}{3} V_{dc} (-s_1 - s_2 + 2s_3) \end{aligned} \quad (26)$$

V_{dc} is DC link voltage of the PWM inverter and s_1, s_2, s_3 switching functions of which value is 0 or 1.

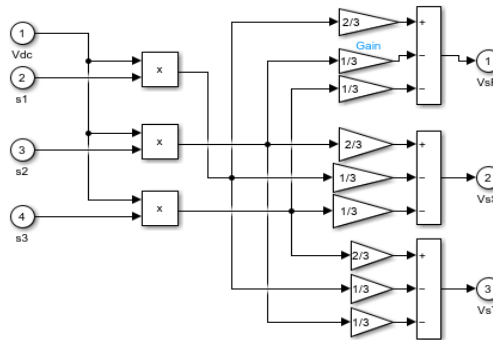


Figure10. Three-phases inverter VSI

3.4. PI controller

A PI controller in (27) serves as a constructive tool in achieving the desired output by adjusting control signals based on the difference between the observed output and the initial goal. By continuously measuring the deviation over time, this technique gradually reduces errors, resulting in precise and accurate control of current and voltage. For a PI controller, the control law is (27).

$$u(t) = K_p e(t) + K_i \int_0^t e(t') dt' \quad (27)$$

Figure 11 shows the employment of the controller in the controlled system, where K_p and K_i are the coefficients of the proportional and integral values, respectively, and $e(t)$ is the measurement error. The goal of the controller is to reduce the error over time by correcting the controlled variable $u(t)$. In our case, some of the inputs can be regulated by the regulator of the fuel cell, such as the regulation of the fuel flow. In addition, we need a voltage regulator for the boosted DC and a regulator for the voltage and current in the inverter.

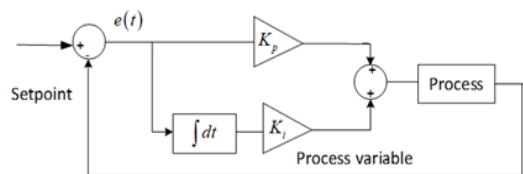


Figure 11. PI controller implementation

3.5. Voltage and current dual regulation

The control method is used for a load-connected inverter, which has two loops - inner loop with current and outer loop with voltage. The aim is to maintain consistent voltage in the DC link while generating a reference current. Control signals for power converters are derived from errors produced in this process, ensuring voltage stability and dynamic reactive power. In off-grid systems, a block that generates a phase angle is used instead of a phase-locked loop.

The dynamic equations for three-phase without resistor damping input and output AC voltage and current inverters [37], [43], [44].

$$\frac{di_{i,abc}}{dt} = \frac{1}{L_1} [V_{i,abc} - R_1 i_{i,abc} - V_{c,abc}] \quad (28)$$

$$\frac{dV_{c,abc}}{dt} = \frac{1}{C_f} [i_{i,abc} - i_{g,abc}] \quad (29)$$

$$\frac{di_{g,abc}}{dt} = \frac{1}{L_2 + L_g} [V_{c,abc} - (R_2 + R_g) i_{g,abc} - V_{g,abc}] \quad (30)$$

The Park dq and Clark transformations can simplify the three-phase system and minimize reciprocal interference, making them suitable for the inverter architecture. The Park transformation is a method used to convert three-phase values into their corresponding $dq0$ quantities, while maintaining the amplitude of the vector simultaneously. The $dq0$ quantity is obtained by converting the three-phase voltage (V_{abc}), current (I_{abc}), or flux (ϕ_{abc}) into their respective values [45].

$$f_{dq0} = [T] f_{abc} = \frac{2}{3} \begin{bmatrix} \cos \theta & \cos \left(\theta - \frac{2\pi}{3} \right) & \cos \left(\theta - \frac{4\pi}{3} \right) \\ -\sin \theta & -\sin \left(\theta - \frac{2\pi}{3} \right) & -\sin \left(\theta - \frac{4\pi}{3} \right) \\ \frac{1}{2} & \frac{1}{2} & \frac{1}{2} \end{bmatrix} f_{abc} \quad (31)$$

Where T the transformation matrix, (θ) is the electrical angle. The inverse Park abc to dq0 is:

$$\begin{bmatrix} \cos \theta & -\sin \theta & 1 \\ \cos \left(\theta - \frac{2\pi}{3} \right) & -\sin \left(\theta - \frac{2\pi}{3} \right) & 1 \\ \cos \left(\theta - \frac{4\pi}{3} \right) & -\sin \left(\theta - \frac{4\pi}{3} \right) & 1 \end{bmatrix} \quad (32)$$

The stationary $\alpha\beta$ frame is transformed to the synchronous $d-q$ frame and vice versa using the following equations:

$$[x_{dq}(t)] = [C] [x_{\alpha\beta}(t)], [C] = \begin{bmatrix} \cos \theta & \sin \theta \\ -\sin \theta & \cos \theta \end{bmatrix} \quad (33)$$

$$[x_{\alpha\beta}(t)] = [C]^{-1} [x_{dq}(t)], [C]^{-1} = \begin{bmatrix} \cos \theta & -\sin \theta \\ \sin \theta & \cos \theta \end{bmatrix} \quad (34)$$

The equation of the stationary abc to $\alpha\beta$ transformation and its inverse transformation, which are used in this paper, are as follows, we used the Clarke method to calculate active and reactive power in the $dq0$ axes are:

$$P = \frac{3}{2} (v_d i_d + v_q i_q) \quad (35)$$

$$Q = \frac{3}{2} (v_q i_d - v_d i_q) \quad (36)$$

The current state variable in the output inverter,

$$\frac{di_{i,d}}{dt} = \omega i_{i,q} + \frac{1}{L_1} [V_{i,d} - R_1 i_{i,d} - V_{c,d}] \quad (37)$$

$$\frac{di_{i,q}}{dt} = -\omega i_{i,d} + \frac{1}{L_1} [V_{i,q} - R_1 i_{i,q} - V_{c,q}] \quad (38)$$

$$\frac{di_{i,o}}{dt} = \frac{1}{L_1} [V_{i,o} - R_1 i_{i,o} - V_{c,o}] \quad (39)$$

The voltage state variable in capacity,

$$\frac{dV_{c,d}}{dt} = \omega V_{c,q} + \frac{1}{C_f} [i_{i,d} - i_{g,d}] \quad (40)$$

$$\frac{dV_{c,q}}{dt} = -\omega V_{c,d} + \frac{1}{C_f} [i_{i,q} - i_{g,q}] \quad (41)$$

$$\frac{dV_{c,o}}{dt} = \frac{1}{C_f} [i_{i,o} - i_{g,o}] \quad (42)$$

The current state variable in the load,

$$\frac{di_{g,d}}{dt} = \omega i_{g,q} + \frac{1}{L_2+L_g} [V_{c,d} - (R_2 + R_g)i_{g,d} - V_{g,d}] \quad (43)$$

$$\frac{di_{g,q}}{dt} = -\omega i_{g,d} + \frac{1}{L_2+L_g} [V_{c,q} - (R_2 + R_g)i_{g,q} - V_{g,q}] \quad (44)$$

$$\frac{di_{g,o}}{dt} = \frac{1}{L_2+L_g} [V_{c,o} - (R_2 + R_g)i_{g,o} - V_{g,o}] \quad (45)$$

The system is symmetrical and balanced, so homopolar sequence components can be neglected.

$$\frac{di_{i,o}}{dt} = 0; \frac{dV_{c,o}}{dt} = 0; \frac{di_{g,o}}{dt} = 0 \quad (46)$$

The variables for the output current and voltage of the inverter and load into dq components are: $i_{i,d}(t)$, $i_{i,q}(t)$, $V_{i,d}(t)$, $V_{i,q}(t)$, $V_{c,d}(t)$, $V_{c,q}(t)$, $i_{g,d}(t)$, $i_{g,q}(t)$, $V_{g,d}(t)$, $V_{g,q}(t)$. The capacitor voltage in the LCL filter is represented by $V_{c,d}(t)$, $V_{c,q}(t)$ while $V_{g,d}(t)$, $V_{g,q}(t)$ represents the load voltage. L_1 and C_f represents the filter inductance and capacitance respectively, and R_g and L_g denote the load resistance and inductance, respectively.

The state-space model for the complete system (37) to (45) might be represented in the following form.

$$\dot{x} = Ax + B_1u_1 + B_2u_2 \quad (47)$$

$$x(t) = [i_{i,d}(t) \ i_{i,q}(t) \ V_{c,d}(t) \ V_{c,q}(t) \ i_{g,d}(t) \ i_{g,q}(t)] \quad (48)$$

$$u_1(t) = [V_{i,d}(t) \ V_{i,q}(t)]^T \quad (49)$$

$$u_2(t) = [V_{g,d}(t) \ V_{g,q}(t)]^T \quad (50)$$

$$y = Cx \quad (51)$$

$$A = \begin{bmatrix} -\frac{R_1}{L_1} & \omega & -\frac{1}{L_1} & 0 & 0 & 0 \\ -\omega & -\frac{R_1}{L_1} & 0 & \frac{1}{L_1} & 0 & 0 \\ \frac{1}{C_f} & 0 & 0 & -\omega & -\frac{1}{C_f} & 0 \\ 0 & \frac{1}{C_f} & \omega & 0 & 0 & -\frac{1}{C_f} \\ 0 & 0 & \frac{1}{L_2+L_g} & 0 & -\frac{R_2+R_g}{L_2+L_g} & \omega \\ 0 & 0 & 0 & \frac{1}{L_2+L_g} & -\omega & -\frac{R_2+R_g}{L_2+L_g} \end{bmatrix} \quad (52)$$

$$B_1 = \begin{bmatrix} \frac{1}{L_1} & 0 \\ 0 & \frac{1}{L_1} \\ 0 & 0 \\ 0 & 0 \\ 0 & 0 \\ 0 & 0 \end{bmatrix} \quad \text{and} \quad B_2 = \begin{bmatrix} 0 & 0 \\ 0 & 0 \\ 0 & 0 \\ -\frac{1}{L_2+L_g} & 0 \\ 0 & -\frac{1}{L_2+L_g} \end{bmatrix} \quad (53)$$

This state-space representation enables the analysis, design, and stability analysis of the inverter system's electrical dynamics and control inputs.

3.5.1. Current controller

The loop that sets the current uses proportional control, which is simpler and gives a faster response during changes to current demand. The current controller (inner loop) presented in Figure 12 for determining the input voltage is modelled as:

The values of $i_{i,d}(t)$ and $i_{i,q}(t)$, are the reference values for the inverter output current in the rotating frame.

$$i_{gdref} = i_{gd} - \omega C_f V_q + \left(k_p + \frac{k_{iV}}{s}\right) (V_{idref} - V_{id}) \quad (54)$$

$$i_{gqref} = i_{gq} - \omega C_f V_{id} + \left(k_{pv} + \frac{k_{iV}}{s}\right) (-V_{iq}) \quad (55)$$

3.5.2. Voltage controller

The voltage loop in Figure 12 contains a proportional-integral (PI) controller that is able to keep the voltage output steady and reduce static error. The state equations are as follows:

$$U_d = -\omega L i_{iq} + \left(k_{pc} + \frac{k_{ic}}{s}\right) (i_{idref} - i_{id}) + V_{id} \quad (56)$$

$$V_q = \omega L i_{id} + \left(k_{pc} + \frac{k_{ic}}{s}\right) (i_{iqref} - i_{iq}) + V_{iq} \quad (57)$$

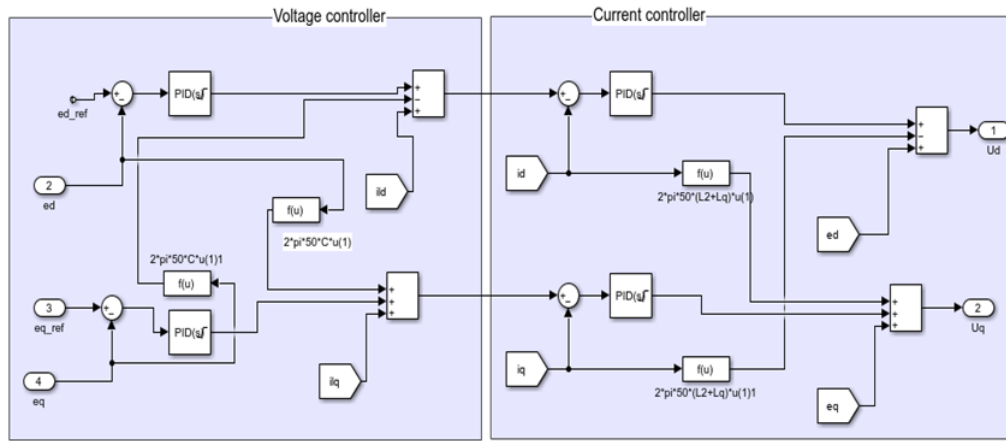


Figure 12. Dual-loop control system for voltage and current regulation

4. RESULTS AND DISCUSSION

Using MATLAB/Simulink software, a computer simulation was conducted for system modeling. Systems with resistive loads were used to test the new system's performance. Figure 13 shows fuel cell parameters, including hydrogen (H_2), water (H_2O), and oxygen (O_2). These parameters can affect the fuel cell efficiency, operating voltage, and current density, among others. The partial pressure of H_2 decreases to 0.0486 atm in time of 0.4 seconds, this lowering is caused by the consumption of hydrogen in the reaction; the partial pressure of H_2O amounts to about 0.8300 atm up to 0.8304 atm this is caused by the production of water vapor continuously; the partial pressure of O_2 decreases over time from 0.04800 atm to 0.04780 atm. This decrease shows that oxygen is also consumed in the reaction. The partial pressures vary relatively small, indicating that the reaction is taking place in a large volume. The load voltage waveform in Figure 14 is sinusoidal, indicating AC power; hence, an alternating current is supplying the load and the current waveform in Figure 15 is also sinusoidal and alternative. A transient period represents a brief time before the current waveform establishes its steady state.

Figure 16 shows active and reactive power. The fluctuation peak of the active power wave directly relates to real power. In contrast, the reactive power wave remains at zero, meaning that the load has no reactive component but is purely resistive. On Figure 17, we can see the DC voltage at the input and output of the DC/DC converter. The output voltage of the fuel cell (FC) is initially higher but remains lower at 400 V, while the output voltage of the boost converter is initially higher but stabilizes around 800 V, which shows an efficient adjustment of the voltage.

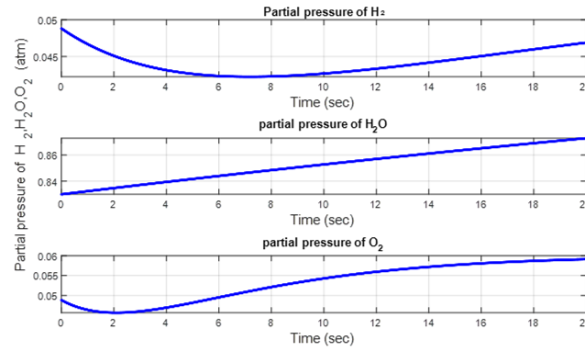
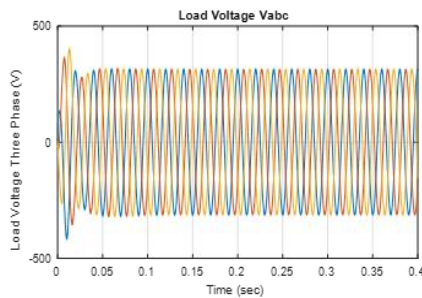
Figure 13. Partial pressures of the gases H_2 , H_2O , and O_2 

Figure 14. Three-voltages in the load

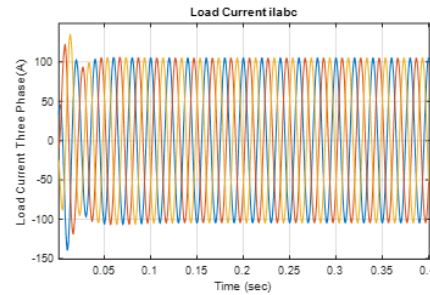


Figure 15. Three-currents in the load

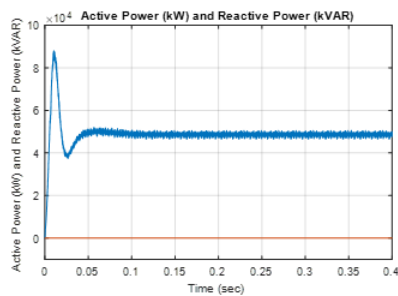


Figure 16. Active and reactive power

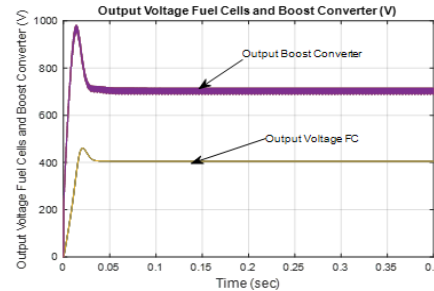


Figure 17. Voltage converter DC/DC

5. CONCLUSION

This study presents a method for developing a high-fidelity dynamic simulation model of a SOFC system using MATLAB/Simulink. The main objective was to model the behavior of the SOFC under stand-alone and off-grid conditions, while developing a complete operational mode applicable to natural systems. The study aimed to solve problems with existing tools and develop new control tools to improve overall system performance. This study examines the power quality of an LCL filter combined with an inverter based on a PI controller.

The results indicate a relatively low total harmonic distortion (THD) for both voltage and current, contributing positively to the system performance parameters. The study indicates that SOFC electricity possesses significant potential; however, it emphasizes the need for a benchmark design and performance to integrate this technology effectively into distributed energy systems. The SOFC model has been utilized to simulate a dynamic off-grid three-phase circuit. The model simulates SOFC operational characteristics and utilizes the fuel cells to satisfy the circuit's energy demands. Recent research indicates that SOFC systems provide distinct advantages for off-grid power generation.

FUNDING INFORMATION

Authors state no funding involved.

AUTHOR CONTRIBUTIONS STATEMENT

This journal uses the Contributor Roles Taxonomy (CRediT) to recognize individual author contributions, reduce authorship disputes, and facilitate collaboration.

Name of Author	C	M	So	Va	Fo	I	R	D	O	E	Vi	Su	P	Fu
Boudjemaa	✓	✓	✓	✓	✓	✓	✓	✓	✓	✓			✓	
Mehimmedetsi														
Abdellah Draidi			✓			✓	✓	✓			✓	✓		✓
Billel Smaani			✓				✓				✓	✓		

C : Conceptualization

M : Methodology

So : Software

Va : Validation

Fo : Formal analysis

I : Investigation

R : Resources

D : Data Curation

O : Writing - Original Draft

E : Writing - Review & Editing

Vi : Visualization

Su : Supervision

P : Project administration

Fu : Funding acquisition

CONFLICT OF INTEREST STATEMENT

Authors state no conflict of interest.

DATA AVAILABILITY

Derived data supporting the findings of this study are available from the corresponding author [Boudjemaa Mehimmedetsi] on request.




REFERENCES

- [1] T. Z. Ang, M. Salem, M. Kamarol, H. S. Das, M. A. Nazari, and N. Prabakaran, "A comprehensive study of renewable energy sources: classifications, challenges and suggestions," *Energy Strategy Reviews*, vol. 43, p. 100939, 2022, doi: 10.1016/j.esr.2022.100939.
- [2] O. Corigliano, L. Pagnotta, and P. Fragiaco, "On the technology of solid oxide fuel cell (SOFC) energy systems for stationary power generation: a review," *Sustainability*, vol. 14, no. 22, p. 15276, Nov. 2022, doi: 10.3390/su142215276.
- [3] Y. S. H. Najjar, "Hydrogen safety: The road toward green technology," *International Journal of Hydrogen Energy*, vol. 38, no. 25, pp. 10716–10728, Aug. 2013, doi: 10.1016/j.ijhydene.2013.05.126.
- [4] H. Li *et al.*, "Safety of hydrogen storage and transportation: an overview on mechanisms, techniques, and challenges," *Energy Reports*, vol. 8, pp. 6258–6269, Nov. 2022, doi: 10.1016/j.egyr.2022.04.067.
- [5] F. S. da Silva and T. M. de Souza, "Novel materials for solid oxide fuel cell technologies: a literature review," *International Journal of Hydrogen Energy*, vol. 42, no. 41, pp. 26020–26036, Oct. 2017, doi: 10.1016/j.ijhydene.2017.08.105.
- [6] A. Kumar Yadav, S. Sinha, and A. Kumar, "Comprehensive review on performance assessment of solid oxide fuel cell-based hybrid power generation system," *Thermal Science and Engineering Progress*, vol. 46, p. 102226, Dec. 2023, doi: 10.1016/j.tsep.2023.102226.
- [7] S. Vora and M. Williams, "The SOFC program at the DOE's office of fossil energy and carbon management (FECM) and national energy technology laboratory (NETL)," *ECS Transactions*, vol. 111, no. 6, pp. 9–14, May 2023, doi: 10.1149/11106.0009ecst.
- [8] B. Reiter, "(Digital Presentation) SOFC - enabler for highly efficient power generation," *ECS Meeting Abstracts*, vol. MA2023-01, no. 40, pp. 2786–2786, Aug. 2023, doi: 10.1149/ma2023-01402786mtgabs.
- [9] B. Yang *et al.*, "Comprehensive summary of solid oxide fuel cell control: a state-of-the-art review," *Protection and Control of Modern Power Systems*, vol. 7, no. 1, p. 36, Dec. 2022, doi: 10.1186/s41601-022-00251-0.
- [10] H. Lai and T. A. Adams, "Life cycle analyses of SOFC/gas turbine hybrid power plants accounting for long-term degradation effects," *Journal of Cleaner Production*, vol. 412, p. 137411, Aug. 2023, doi: 10.1016/j.jclepro.2023.137411.
- [11] Y. Liu *et al.*, "A novel adaptive model predictive control strategy of solid oxide fuel cell in DC microgrids," *IEEE Transactions on Industry Applications*, vol. 58, no. 5, pp. 6639–6654, Sep. 2022, doi: 10.1109/TIA.2022.3180971.
- [12] D. Shin, T. Kim, and S. Kang, "Design and performance analysis of a cascade solid oxide fuel cell system for high electrical efficiency," *Applied Thermal Engineering*, vol. 195, p. 117214, Aug. 2021, doi: 10.1016/j.applthermaleng.2021.117214.
- [13] G. Brunaccini *et al.*, "Modeling of a SOFC-HT battery hybrid system for optimal design of off-grid base transceiver station," *International Journal of Hydrogen Energy*, vol. 42, no. 46, pp. 27962–27978, Nov. 2017, doi: 10.1016/j.ijhydene.2017.09.062.
- [14] L. Tan, X. Dong, C. Chen, Z. Gong, and M. Wang, "Diverse system layouts promising fine performance demonstration: a comprehensive review on present designs of SOFC-based energy systems for building applications," *Energy Conversion and Management*, vol. 245, p. 114539, Oct. 2021, doi: 10.1016/j.enconman.2021.114539.
- [15] F. Baldi, L. Wang, M. Pérez-Fortes, and F. Maréchal, "A cogeneration system based on solid oxide and proton exchange membrane fuel cells with hybrid storage for off-grid applications," *Frontiers in Energy Research*, vol. 6, Jan. 2019, doi: 10.3389/fenrg.2018.00139.
- [16] A. Gelen and T. Yalcinoz, "The modeling and simulation of thermal based modified solid oxide fuel cell (SOFC) for grid-connected systems," *Acta Scientiarum. Technology*, vol. 37, no. 2, p. 211, May 2015, doi: 10.4025/actascitechnol.v37i2.24941.
- [17] K. Ro and S. Rahman, "Control of grid-connected fuel cell plants for enhancement of power system stability," *Renewable Energy*, vol. 28, no. 3, pp. 397–407, Mar. 2003, doi: 10.1016/S0960-1481(02)00042-3.
- [18] Y. H. Li, S. Rajakaruna, and S. S. Choi, "Control of a solid oxide fuel cell power plant in a grid-connected system," *IEEE Transactions on Energy Conversion*, vol. 22, no. 2, pp. 405–413, Jun. 2007, doi: 10.1109/TEC.2005.853756.
- [19] F. Sergi *et al.*, "PEM fuel cells analysis for grid connected applications," *International Journal of Hydrogen Energy*, vol. 36, no. 17, pp. 10908–10916, Aug. 2011, doi: 10.1016/j.ijhydene.2011.05.161.




- [20] M. Singh, D. Zappa, and E. Comini, "Solid oxide fuel cell: decade of progress, future perspectives and challenges," *International Journal of Hydrogen Energy*, vol. 46, no. 54, pp. 27643–27674, Aug. 2021, doi: 10.1016/j.ijhydene.2021.06.020.
- [21] F. Lefebvre-Joud, L. Antoni, N. Bardi, O. Lemaire, and F. L. N. et J. Mougin, "Fuel cells technology: which may be the winners?," Commissariat à l'Energie Atomique et aux Energies Alternatives (CEA). Accessed: Jan. 04, 2024. [Online]. Available: https://www.college-de-france.fr/media/jean-marie-tarascon/UPL18091_Piles____combustible_FLJ_NXPowerLite_.pdf
- [22] K. Wang *et al.*, "A review on solid oxide fuel cell models," *International Journal of Hydrogen Energy*, vol. 36, no. 12, pp. 7212–7228, Jun. 2011, doi: 10.1016/j.ijhydene.2011.03.051.
- [23] E. Bompard, R. Napoli, G. Orsello, D. Roïu, A. Tenconi, and B. Wan, "Technical considerations of SOFCs for mixed DG/backup power applications," *International Journal of Hydrogen Energy*, vol. 33, no. 22, pp. 6743–6748, Nov. 2008, doi: 10.1016/j.ijhydene.2008.05.109.
- [24] F. Zabihian and A. Fung, "Advanced power generation technologies: fuel cells," in *Paths to Sustainable Energy*, 2010, doi: 10.5772/13373.
- [25] A. Erdogan, F. Capotondo, A. C. Ince, A. Hagen, and C. O. Colpan, "Analysis of reformat syngas mixture fed solid oxide fuel cell through experimental and 0-D thermodynamic modeling studies," *International Journal of Hydrogen Energy*, vol. 48, no. 60, pp. 23110–23126, Jul. 2023, doi: 10.1016/j.ijhydene.2022.10.139.
- [26] R. O'hayre, S.-W. Cha, W. Colella, and F. B. Prinz, "Fuel cell fundamentals," in *John Wiley & Sons*, 2016.
- [27] H. Mahcene, H. Ben Moussa, H. Bouguettaia, D. Bechki, S. Babay, and M. S. Meftah, "Study of species, temperature distributions and the solid oxide fuel cells performance in a 2-D model," *International Journal of Hydrogen Energy*, vol. 36, no. 6, pp. 4244–4252, Mar. 2011, doi: 10.1016/j.ijhydene.2010.07.075.
- [28] H. Yakabe, T. Ogiwara, M. Hishinuma, and I. Yasuda, "3-D model calculation for planar SOFC," *Journal of Power Sources*, vol. 102, no. 1–2, pp. 144–154, Dec. 2001, doi: 10.1016/S0378-7753(01)00792-3.
- [29] M. Nerat and D. Juričić, "A comprehensive 3-D modeling of a single planar solid oxide fuel cell," *International Journal of Hydrogen Energy*, vol. 41, no. 5, pp. 3613–3627, Feb. 2016, doi: 10.1016/j.ijhydene.2015.11.136.
- [30] A. C. Lazanas and M. I. Prodromidis, "Electrochemical impedance spectroscopy-a tutorial," *ACS Measurement Science Au*, vol. 3, no. 3, pp. 162–193, Jun. 2023, doi: 10.1021/acsmesuresciau.2c00070.
- [31] U. Pasaogullari and C.-Y. Wang, "Computational fluid dynamics modeling of solid oxide fuel cells," *ECS Proceedings Volumes*, vol. 2003–07, no. 1, pp. 1403–1412, Jan. 2003, doi: 10.1149/200307.1403pv.
- [32] J. Padullés, G. W. Ault, and J. R. McDonald, "Integrated SOFC plant dynamic model for power systems simulation," *Journal of Power Sources*, vol. 86, no. 1, pp. 495–500, Mar. 2000, doi: 10.1016/S0378-7753(99)00430-9.
- [33] Y. Zhu and K. Tomsovic, "Development of models for analyzing the load-following performance of microturbines and fuel cells," *Electric Power Systems Research*, vol. 62, no. 1, pp. 1–11, May 2002, doi: 10.1016/S0378-7796(02)00033-0.
- [34] S. A. Hajimolana, M. A. Hussain, W. M. A. W. Daud, M. Soroush, and A. Shamiri, "Mathematical modeling of solid oxide fuel cells: a review," *Renewable and Sustainable Energy Reviews*, vol. 15, no. 4, pp. 1893–1917, May 2011, doi: 10.1016/j.rser.2010.12.011.
- [35] A. Safari, H. Shahsavari, and F. Babaei, "Optimal design of controllers for power network connected SOFC using of multi-objective PSO," *Serbian Journal of Electrical Engineering*, vol. 15, no. 2, pp. 145–163, 2018, doi: 10.2298/sjee170822001s.
- [36] J. Milewski, M. Santarelli, K. Świrski, and P. Leo, "Advanced methods of solid oxide fuel cell modeling," in *Springer Science & Business Media*, vol. 40, 2011.
- [37] S.-W. Seo and H. H. Choi, "Digital implementation of fractional order PID-type controller for boost DC–DC converter," *IEEE Access*, vol. 7, pp. 142652–142662, 2019, doi: 10.1109/ACCESS.2019.2945065.
- [38] X. J. Wu, X. J. Zhu, G. Y. Cao, and H. Y. Tu, "Predictive control of SOFC based -n a GA-RBF neural network model," *Journal of Power Sources*, vol. 179, no. 1, pp. 232–239, Apr. 2008, doi: 10.1016/j.jpowsour.2007.12.036.
- [39] M. Liserre, F. Blaabjerg, and S. Hansen, "Design and control of an LCL-filter-based three-phase active rectifier," *IEEE Transactions on Industry Applications*, vol. 41, no. 5, pp. 1281–1291, Sep. 2005, doi: 10.1109/TIA.2005.853373.
- [40] K. A. El Wahid Hamza, L. Hassaine, and L. Cherif, "LCL filter design with passive damping for photovoltaic grid connected systems," in *2015 6th International Renewable Energy Congress, IREC 2015*, IEEE, Mar. 2015, pp. 1–4, doi: 10.1109/IREC.2015.7110945.
- [41] M. Y. Park, M. H. Chi, J. H. Park, H. G. Kim, T. W. Chun, and E. C. Nho, "LCL-filter design for grid-connected PCS using total harmonic distortion and ripple attenuation factor," in *2010 International Power Electronics Conference - ECCE Asia -, IPEC 2010*, IEEE, Jun. 2010, pp. 1688–1694, doi: 10.1109/IPEC.2010.5542131.
- [42] A. M. Trzynadlowski, "Introduction to modern power electronics," in *John Wiley & Sons*, 2015.
- [43] F. D. Mohammadi, H. K. Vanashi, and A. Feliachi, "State-space modeling, analysis, and distributed secondary frequency control of isolated microgrids," *IEEE Transactions on Energy Conversion*, vol. 33, no. 1, pp. 155–165, Mar. 2018, doi: 10.1109/TEC.2017.2757012.
- [44] N. Pogaku, M. Prodanović, and T. C. Green, "Modeling, analysis and testing of autonomous operation of an inverter-based microgrid," *IEEE Transactions on Power Electronics*, vol. 22, no. 2, pp. 613–625, Mar. 2007, doi: 10.1109/TPEL.2006.890003.
- [45] C. J. O'Rourke, M. M. Qasim, M. R. Overlin, and J. L. Kirtley, "A geometric interpretation of reference frames and transformations: dq0, Clarke, and Park," *IEEE Transactions on Energy Conversion*, vol. 34, no. 4, pp. 2070–2083, Dec. 2019, doi: 10.1109/TEC.2019.2941175.

BIOGRAPHIES OF AUTHORS






Dr. Boudjemaa Mehimmedetsi    received the Electromechanical Engineer degree from University of Annaba, Algeria, in 1992 and the Magister and Doctorate degrees in electrotechnics in 2008 and 2018 respectively from the Department of Electrotechnics, University of Constantine 1, Algeria. Currently, he is a lecturer at the Electromechanical Department, University of MILA, Algeria. His research interests include renewable energy, power systems, hybrid power systems, control of electrical machines. He can be contacted at email: mehim.boudj@gmail.com or b.mehimmedetsi@centre-univ-mila.dz.



Abdellah Draidi    received the Engineer degree in electrotechnics from University of Constantine 1, Algeria, in 2006 and the Magister and Doctorate degrees in Electrotechnics in 2010 and 2016 respectively from the Department of Electrotechnics, University of Constantine 1, Algeria. Currently, he is a lecturer and Head of the Electromechanical department at the Institute of Applied Science and Technology (Institut des sciences et techniques appliquées ISTA), University of Constantine 1, Algeria. His research interests include renewable energy, power systems, load flow control, economic dispatch, artificial intelligence techniques, and industrial automation. He can be contacted at email: draidi_abdelh@umc.edu.dz or abdellah.draidi@gmail.com.



Billel Smaani    received the Ph.D. degrees from the University of Frère Mentouri, Constantine, Algeria, in 2015. He joined the Centre Universitaire Abdelhafid Boussouf Mila, Algeria, in 2021, where he has been an Associate Professor since June 2022. From 2015 to 2021, he was with the University of M'hamed Bougara Boumerdes, Algeria. His current research interests include study, analysis and compact modeling of advanced nanoscale field-effect transistors for analog and digital circuits co-design. He can be contacted at email: billel.smaani@gmail.com.